

The competition between the hydrodynamic instability from noise and magnetorotational instability in the Keplerian disks

Subham Ghosh^{1, a)} and Banibrata Mukhopadhyay^{1, b)}

Department of Physics, Indian Institute of Science, Bangalore 560012, India

We venture for the comparison between growth rates for magnetorotational instability (MRI) and hydrodynamics instability in the presence of an extra force in the local Keplerian accretion flow. The underlying model is described by the Orr-Sommerfeld and Squire equations in the presence of rotation, magnetic field and an extra force, plausibly noise with a nonzero mean. We obtain MRI using Wentzel-Kramers-Brillouin (WKB) approximation without extra force for purely vertical magnetic field and vertical wavevector of the perturbations. Expectedly, MRI is active within a range of magnetic field, which changes depending on the perturbation wavevector magnitude. Next, to check the effect of noise on the growth rates, a quartic dispersion relation has been obtained. Among those four solutions for growth rate, the one that reduces to MRI growth rate at the limit of vanishing mean of noise in the MRI active region of the magnetic field, is mostly dominated by MRI. However, in MRI inactive region, in the presence of noise the solution turns out to be unstable, which are almost independent of the magnetic field. Another growth rate, which is almost complementary to the previous one, leads to stability at the limit of vanishing noise. The remaining two growth rates, which correspond to the hydrodynamical growth rates at the limit of the vanishing magnetic field, are completely different from the MRI growth rate. More interestingly, the latter growth rates are larger than that of the MRI. If we consider viscosity, the growth rates decrease depending on the Reynolds number.

I. INTRODUCTION

The accretion disk is one of the exotic objects in Astrophysics. As the name suggests, they form in a disk-like shape due to the accretion of matter with angular momentum around a center by unleashing enormous gravitational energy through radiation. They are ubiquitous. From around the center of the galaxies to the formation of planets, from the binary system to the ring of Saturn, they prevail at various length scales. The physics related to the accretion disks is also exotic. There have been a lot of studies regarding the phenomena related to the accretion disks, and it still continues. However, still there are some open questions in the field of accretion disks. One of those is how, in the first place, the accretion disk forms, i.e., how the matter falls in, losing the angular momentum and eventually reaches the central object, particularly where the molecular viscosity is negligible. We attempt to address this question in this work.

To match with the observational evidences¹, the accretion flow has to be turbulent². However, the accretion flow in the Keplerian accretion disk, where the centrifugal force almost balances the gravity, is Rayleigh (centrifugally) stable, i.e., the infinitesimal perturbation eventually dies down. The route to turbulence, therefore, is essential to find. In 1991, Balbus and Hawley³ proposed the idea of an ideal magnetohydrodynamical (MHD) instability following Velikhov⁴ and Chandrasekhar⁵: magnetorotational instability (MRI). The interplay between the weak magnetic field and the rotation of the fully ionized plasma gives rise to the MRI. It is a widespread

mechanism in leading to turbulence and explaining the transport of angular momentum in accretion disks. This is because it grows within the dynamical timescale with very minimum requirements: weak magnetic field so that the corresponding magnetic pressure is smaller than the hydrodynamical pressure, and a radially decreasing angular velocity in contrast to the radially decreasing specific angular momentum as the Rayleigh stability criterion⁶. Despite of its popularity in the accretion disk community and tremendous success in explaining various accretion phenomena over the years, the MRI is not out of caveats. When the temperature is low, the fluid and the magnetic field do not get coupled well due to inefficient ionization. Consequently, the nonideal MHD effects come into the picture. Due to the stabilizing effects of Ohmic resistivity on the linear instability, there are many regions in protoplanetary disks where MRI gets suppressed^{7,8}. The additional inclusion of ambipolar diffusion makes this scenario worse⁹.

In order to explain the angular momentum transport, magnetised disk winds have been considered as an alternative to MRI turbulence^{10,11}. If the toroidal component of the magnetic field is beyond the critical value, MRI gets suppressed locally¹² and globally¹³. Instead, there arise different MHD instabilities. Moreover, due to the nonnormality of the underlying system, it has been argued that the magnetic transient growth¹⁴ brings nonlinearly and hence plausible turbulence faster than MRI for the flows with the Reynolds number (Re) beyond 10^9 . Since Re in accretion disk¹⁵ is much larger than this value, MRI is questionable in systems with large Re . It, therefore, would be an enthralling venture to look for the instability mechanisms of hydrodynamical origins.

A lot of efforts have been put forward to understand the angular momentum transport in accretion disks in the laboratory, i.e., through the table top experiments

^{a)}subham@iisc.ac.in

^{b)}bm@iisc.ac.in

and simulations. To do so, the accretion disk-like environment, i.e., the Keplerian angular velocity, has been created in the experiments. In the experimental context, the Taylor-Couette flow¹⁶ has been considered. Its crude description is the following. It has two concentric cylinders and fluid in between. By moving the cylinders, the fluid is kept in motion. The flow parameters, i.e., the velocity, angular velocity, Re , etc., are controlled by the speed of both the cylinders¹⁷. Although the exploration of the transport of angular momentum in accretion disk through laboratory started by Richard and Zahn¹⁸ in 1999, based on the key experimental results, there are mainly two groups in the community: one (Group 1) who obtained hydrodynamic turbulence^{19–21} for the Keplerian angular velocity profile and the other one (Group 2) who did not obtain any hydrodynamic turbulence²² for the same. All the experiments reached the equivalently same Re to draw their conflicting conclusions. Although they obtained the same Re , the two groups have different experimental devices. Group 1 did the experiment with a tall and narrow device, while Group 2 used a small and wide apparatus. These kinds of geometrical differences in the apparatus affect the critical Re of the corresponding flows remarkably^{18,23}. For the same reason, turbulence is hard to reach in the case of wide apparatus. It could be plausible for Group 2 that they operated the apparatus at the verge of the critical Re required for the transition to turbulence or below the critical Re so that they did not reach the turbulent regime. Although, in reality, there is no rigid axial boundary in accretion disks, due to the finite size of the apparatus, each group differently implemented the axial boundaries. To check the effect of these axial boundaries on the flow, a direct numerical simulation²⁴, with very small Re compared to the experiments due to the computational constraint, was performed in the equivalent set up of the experiments done by both the groups. The simulations of both the experiments show that the flows become turbulent mainly due to the presence of the boundaries. Hence, the effects of boundaries, i.e., the finite size of the apparatus have important roles in bringing turbulence. From the theoretical, numerical, and experimental points of view, the current status of the field is still far from settling down.

Keeping in mind the nonmagnetic Keplerian flow, an alternative approach of linear transient growth^{25–29} has been also proposed. Due to the non-selfadjoint property of the underlying differential operator, the total energy³⁰ of the linear perturbations in the shear flow becomes significantly large for a short time before their eventual decay. Although its tremendous success is in explaining the subcritical transition to turbulence in the laboratory shear flows, authors^{28,31,32} questioned for the corresponding sustained turbulence in the Keplerian flow. However, several orders of magnitude discrepancies exist between the current computational resolution and the Re of the accretion disk. Nevertheless, we encounter the problem from the hydrodynamical point of view but in the presence of an extra force. Considering this extra

force to be the white noise with a zero mean, the multi-mode analysis of the Keplerian flow has been studied^{33,34}. We instead follow the idea and methodology put forwarded by Mukhopadhyay and Chattopadhyay¹⁵. Recently, authors^{35–38} argued that if the white noise has a nonzero mean, the Keplerian flow effectively becomes linearly unstable. The origin of the extra force in the context of accretion flow, as merely mentioned by Ioannou and Kakouris³³, could be the neglected nonlinear terms during the linear analysis, supernova explosions, etc. However, the other plausible models for its origin, as proposed explicitly and rigorously by Ghosh and Mukhopadhyay³⁶ very recently, could be the dust-grain interaction in protoplanetary disks, feedback from the outflow/jet on the accretion disks, etc. Nevertheless, the comparison between the growth rates of hydrodynamical instability in the presence of an extra force and that of the MRI has never been studied. Although there could be different models for the extra force^{33,36}, we however, restrict ourselves to the white noise with nonzero mean as the extra force in this work. This study has its own significance because the presence of noise is not limited^{35,36} to the nonmagnetic Keplerian flow. The presence of noise, in fact, is quite ubiquitous in any Keplerian flow as argued by Nath and Mukhopadhyay³⁵ and later Ghosh and Mukhopadhyay³⁶. Hence, it is very important to compare these two growth rates to check whether they come in unison, or one opposes the other. In other words, what the growth rate corresponding to the hydrodynamical instability is in the favorable parameter space for MRI. If the growth rate of the hydrodynamical instability is comparable to that of the MRI, we can say that irrespective of the magnetic field, the accretion flow is linearly unstable. Hence, nonlinearity and turbulence eventually could be the inevitable fate of the magnetic or nonmagnetic Keplerian flow.

The decoration of the paper is the following. In §II, we first formulate the problem in the local shearing box situated at a local patch of the accretion disk. In the local box, the governing equations to describe the linearly perturbed background flow are the magnetic Orr-Sommerfeld and Squire equations in the presence of an extra force and the Coriolis force. The corresponding background magnetic and velocity fields are also described here. With these equations, in the absence of the extra force, we obtain a dispersion relation neglecting the hydrodynamic and magnetic viscosities to obtain the criteria for centrifugal instability (CI) and MRI in §III. The effect of the force is described in §IV, where the dispersion relation in the presence of noise but in the absence of any kinds of viscosity is obtained. Note that if the external force is not stochastic rather deterministic, similar scenario can also be implemented. The solutions for that dispersion relation have been studied extensively without magnetic field in §IV A and with magnetic field in §IV B. In §V, we include the effect of the hydrodynamic viscosity on the growth rates. We conclude in §VI that depending on the extra force, the hydrodynamic growth rate in the

favorable parameter zone for MRI becomes greater than that of the MRI. For other parameters, which lead to the suppression of MRI, it is the hydrodynamical instability that makes the flow unstable and plausibly further turbulent. Hence, the presence of noise in the flow is enough to make the underlying flow unstable.

II. FORMALISM

We refer to the local patch of the Keplerian accretion disk, where we do the whole analysis. For the detailed description of the local formulation, please see^{28,39,40}. The governing equations of the perturbed flow are magnetic Navier-Stokes equation in the presence of rotation and noise, the magnetic induction equation with the constraints of incompressibility^{14,29} due to the local nature of the flow, and the no-magnetic monopole. We, however, recast the governing equations into magnetic Orr-Sommerfeld and Squire equations (see Appendix of Mukhopadhyay and Chattopadhyay¹⁵ for the detailed derivation). The background and perturbed velocities are $\mathbf{U}_0 = (0, -x, 0)$ ^{6,28,38} and (u, v, w) , respectively. For the present purpose, the background and perturbed magnetic fields are $\mathbf{B}_0 = (B_{0x}, B_{0y}, B_{0z})$ and (B_x, B_y, B_z) , respectively. Hence, taking into account the above mentioned background and perturbed quantities, the magnetized Orr-Sommerfeld and Squire equations become

$$\left(\frac{\partial}{\partial t} - x \frac{\partial}{\partial y}\right) \nabla^2 u + \frac{2}{q} \frac{\partial \zeta}{\partial z} - \frac{1}{4\pi} (\mathbf{B}_0 \cdot \nabla) \nabla^2 B_x = \frac{1}{Re} \nabla^4 u + \eta_1, \quad (1a)$$

$$\left(\frac{\partial}{\partial t} - x \frac{\partial}{\partial y}\right) \zeta + \left(1 - \frac{2}{q}\right) \frac{\partial u}{\partial z} - \frac{1}{4\pi} (\mathbf{B}_0 \cdot \nabla) \zeta_B = \frac{1}{Re} \nabla^2 \zeta + \eta_2, \quad (1b)$$

$$\left(\frac{\partial}{\partial t} - x \frac{\partial}{\partial y}\right) B_x - (\mathbf{B}_0 \cdot \nabla) u = \frac{1}{Rm} \nabla^2 B_x, \quad (1c)$$

$$\left(\frac{\partial}{\partial t} - x \frac{\partial}{\partial y}\right) \zeta_B - (\mathbf{B}_0 \cdot \nabla) \zeta - \frac{\partial}{\partial z} B_x = \frac{1}{Rm} \nabla^2 \zeta_B, \quad (1d)$$

where $\eta_{1,2}$ are the extra force; $\zeta = \partial w / \partial y - \partial v / \partial z$ and $\zeta_B = \partial B_z / \partial y - \partial B_y / \partial z$ are the x -component of vorticity and magnetic vorticity, respectively; Re and Rm are the Reynolds and magnetic Reynolds numbers, respectively; q is the rotation parameter describing the radial dependence (r) of the angular frequency (Ω) of fluid element around the central object, given by $\Omega \propto r^{-q}$.

We have to write down all the equations (1a), (1b), (1c) and (1d) in the Fourier space in the due course of

calculation. For that our convention of the Fourier transformation and the inverse Fourier transformation are respectively,

$$A(\mathbf{r}, t) = \int \tilde{A}_{\mathbf{k}, \omega} e^{i(\mathbf{k} \cdot \mathbf{r} - \omega t)} d^3 k d\omega \quad (2a)$$

and

$$\tilde{A}_{\mathbf{k}, \omega} = \left(\frac{1}{2\pi}\right)^4 \int A(\mathbf{r}, t) e^{-i(\mathbf{k} \cdot \mathbf{r} - \omega t)} d^3 x dt, \quad (2b)$$

where A can be any one of $u, \zeta, B_x, \zeta_B, \eta_1$ and η_2 ; \mathbf{k} and ω are the wavevector and the corresponding frequency of the perturbation in the Fourier space such that in Cartesian coordinates $\mathbf{k} \equiv (k_x, k_y, k_z)$ and $|\mathbf{k}| = k$; \mathbf{r} is the position vector and in Cartesian coordinates $\mathbf{r} \equiv (x, y, z)$.

The boundary conditions to solve equations (1a), (1b), (1c) and (1d) are

$$u = \frac{\partial u}{\partial x} = \zeta = B_x = \frac{\partial B_x}{\partial x} = \zeta_B = 0, \text{ at } x = \pm 1. \quad (3)$$

In the Fourier space, the above equations reduce to

$$\begin{aligned} -k_y k^2 \frac{\partial \tilde{u}_{\mathbf{k}, \omega}}{\partial k_x} + \left(i\omega k^2 - 2k_x k_y - \frac{k^4}{Re}\right) \tilde{u}_{\mathbf{k}, \omega} \\ + \frac{2ik_z}{q} \tilde{\zeta}_{\mathbf{k}, \omega} + \frac{ik^2}{4\pi} (\mathbf{B}_0 \cdot \mathbf{k}) \tilde{B}_{x; \mathbf{k}, \omega} = m_1 \delta(\mathbf{k}) \delta(\omega), \end{aligned} \quad (4a)$$

$$\begin{aligned} k_y \frac{\partial \tilde{\zeta}_{\mathbf{k}, \omega}}{\partial k_x} + ik_z \left(1 - \frac{2}{q}\right) \tilde{u}_{\mathbf{k}, \omega} + \left(\frac{k^2}{Re} - i\omega\right) \tilde{\zeta}_{\mathbf{k}, \omega} \\ - \frac{i}{4\pi} (\mathbf{B}_0 \cdot \mathbf{k}) \tilde{\zeta}_{B; \mathbf{k}, \omega} = m_2 \delta(\mathbf{k}) \delta(\omega), \end{aligned} \quad (4b)$$

$$\begin{aligned} k_y \frac{\partial}{\partial k_x} \tilde{B}_{x; \mathbf{k}, \omega} + \left(\frac{k^2}{Rm} - i\omega\right) \tilde{B}_{x; \mathbf{k}, \omega} \\ - i(\mathbf{B}_0 \cdot \mathbf{k}) \tilde{u}_{\mathbf{k}, \omega} = 0, \end{aligned} \quad (4c)$$

$$\begin{aligned} k_y \frac{\partial}{\partial k_x} \tilde{\zeta}_{B; \mathbf{k}, \omega} + \left(\frac{k^2}{Rm} - i\omega\right) \tilde{\zeta}_{B; \mathbf{k}, \omega} \\ - i(\mathbf{B}_0 \cdot \mathbf{k}) \tilde{\zeta}_{\mathbf{k}, \omega} - ik_z \tilde{B}_{x; \mathbf{k}, \omega} = 0. \end{aligned} \quad (4d)$$

We choose the solutions of the equations (1a), (1b), (1c) and (1d) be $\psi = \psi(x) e^{i(\boldsymbol{\alpha} \cdot \mathbf{r} - \beta t)}$, where ψ can be any of u, ζ, B_x and ζ_B ; $\boldsymbol{\alpha} = (\alpha_1, \alpha_2, \alpha_3)$ is the wave vector, β is the frequency. In general, β is complex. However, according to our convention, if the imaginary part of β , i.e., $Im(\beta)$ is positive, then the perturbation grows with time and hence makes the flow unstable. In the Fourier space, these solutions become

$$\begin{aligned} \tilde{\psi}_{\mathbf{k}, \omega} &= \left(\frac{1}{2\pi}\right)^4 \int_{-\infty}^{\infty} \psi(x) e^{i(\boldsymbol{\alpha} \cdot \mathbf{r} - \beta t)} e^{-i(\mathbf{k} \cdot \mathbf{r} - \omega t)} d^3 x dt \\ &= \frac{1}{2\pi} \delta(\alpha_2 - k_y) \delta(\alpha_3 - k_z) \delta(\beta - \omega) \int_{-\infty}^{\infty} \psi(x) e^{i(\alpha_1 - k_x)x} dx. \end{aligned}$$

To obtain the dispersion relation, we integrate the equations (4a), (4b), (4c) and (4d) with respect to \mathbf{k} and ω and obtain the following equations. In the due process, we have neglected the second and higher order derivatives. Thence the corresponding equations are

$$\begin{aligned} & \left(i\beta\alpha^2 - \frac{\alpha^4}{Re} \right) u(0) + 2i\alpha_1 \left(\frac{2\alpha^2}{Re} - i\beta \right) u'(0) \\ & + \frac{2i\alpha_3}{q} \zeta(0) + \frac{i}{4\pi} [(\mathbf{B}_0 \cdot \boldsymbol{\alpha})(\alpha^2 B_x(0) - 2i\alpha_1 B'_x(0))] \\ & = m_1, \end{aligned} \quad (5a)$$

$$\begin{aligned} & i\alpha_3 \left(1 - \frac{2}{q} \right) u(0) + \left(\frac{\alpha^2}{Re} - i\beta \right) \zeta(0) - \frac{2i\alpha_1}{Re} \zeta'(0) \\ & - \frac{i}{4\pi} (\mathbf{B}_0 \cdot \boldsymbol{\alpha}) \zeta_B(0) = m_2, \end{aligned} \quad (5b)$$

$$\begin{aligned} & \left(\frac{\alpha^2}{Rm} - i\beta \right) B_x(0) - \frac{2i\alpha_1}{Rm} B'_x(0) \\ & - i(\mathbf{B}_0 \cdot \boldsymbol{\alpha}) u(0) = 0, \end{aligned} \quad (5c)$$

$$\begin{aligned} & \left(\frac{\alpha^2}{Rm} - i\beta \right) \zeta_B(0) - \frac{2i\alpha_1}{Rm} \zeta'_B(0) \\ & - i(\mathbf{B}_0 \cdot \boldsymbol{\alpha}) \zeta(0) - i\alpha_3 B_x(0) = 0. \end{aligned} \quad (5d)$$

A. Background magnetic field

Before proceeding further, we have to specify the background magnetic field, B_0 , like we know about U_0 . The induction equation in dimensionless unit, in general, is

$$\frac{\partial \mathbf{B}}{\partial t} = \nabla \times (\mathbf{V} \times \mathbf{B}) + \frac{1}{Rm} \nabla^2 \mathbf{B}, \quad (6)$$

where \mathbf{B} and \mathbf{V} are arbitrary magnetic and velocity field vectors respectively. If we assume the background magnetic field to be constant over space and time, then equation (6) for background quantities becomes

$$\nabla \times (\mathbf{U}_0 \times \mathbf{B}_0) = (\mathbf{B}_0 \cdot \nabla) \mathbf{U}_0 - (\mathbf{U}_0 \cdot \nabla) \mathbf{B}_0 = 0. \quad (7)$$

For $\mathbf{U}_0 = (0, -x, 0)$, the equation (7) becomes

$$-B_{0x} \mathbf{j} + x \frac{\partial \mathbf{B}_0}{\partial y} = 0, \quad (8)$$

where \mathbf{j} is the unit vector along the y -direction in Cartesian coordinates. We, therefore, obtain that for constant background magnetic field, $B_{0x} = 0$, hence, $\mathbf{B}_0 = (0, B_{0y}, B_{0z})$. In this work, we shall be however focusing on the vertical magnetic field, i.e. $\mathbf{B}_0 = (0, 0, B_{0z})$.

III. THE CENTRIFUGAL INSTABILITY AND MAGNETOROTATIONAL INSTABILITY

It is always interesting to obtain CI and MRI following our formalism. We, in fact, obtain the corresponding dispersion relations out of equations (5a), (5b), (5c) and (5d) omitting noise. Our primary interest is for vertical wave vector, i.e., $\boldsymbol{\alpha} = (0, 0, \alpha_3)$. We also neglect the effect of viscosity for the time being. Eventually, in this work itself, we include all of them one by one in the due course of study. Considering all these, equations (5a), (5b), (5c) and (5d) become

$$\begin{aligned} & i\beta\alpha_3^2 u(0) + \frac{2i\alpha_3}{q} \zeta(0) + \frac{i\alpha_3^3 B_{0z} B_x(0)}{4\pi} = 0, \\ & i\alpha_3 \left(1 - \frac{2}{q} \right) u(0) - i\beta \zeta(0) - \frac{i}{4\pi} B_{0z} \alpha_3 \zeta_B(0) = 0, \quad (9) \\ & -i\beta B_x(0) - iB_{0z} \alpha_3 u(0) = 0, \\ & -i\beta \zeta_B(0) - iB_{0z} \alpha_3 \zeta(0) - i\alpha_3 B_x(0) = 0. \end{aligned}$$

For the nontrivial solutions of the above system of linear equations, we obtain the following dispersion relation

$$\begin{aligned} & 16\pi^2 \beta^4 - 8\pi \left[B_{0z}^2 \alpha_3^2 - \left(4\pi \left(\frac{1}{q} - \frac{2}{q^2} \right) \right) \right] \beta^2 \\ & + B_{0z}^4 \alpha_3^4 - \frac{8\pi B_{0z}^2 \alpha_3^2}{q} = 0. \end{aligned} \quad (10)$$

For the centrifugal instability^{16,41}, we get rid of the magnetic field from the equation (10). The nontrivial solutions are

$$\beta = \pm \frac{\sqrt{2}}{q} \sqrt{2 - q}. \quad (11)$$

It tells us that for $q > 2$, the flow becomes unstable. If we keep the magnetic field and get rid of the rotation parameter (q), we would obtain magneto-hydrodynamical (MHD) waves with frequency

$$\beta = \pm \frac{B_{0z} \alpha_3}{2\sqrt{\pi}}. \quad (12)$$

This waves are called Alfvén wave with Alfvén speed, $V_A = B_{0z}/2\sqrt{\pi}$.

If we keep both rotation as well as the magnetic field, from the equation (10), we obtain that $q > 0$ for instability, i.e., negative β^2 for an arbitrarily small α_3 . This is MRI. Equation (10) shows that β has four solutions. However, among them only one provides instability. FIG. 1 shows the variation of $Im(\beta)$ as a function of B_{0z} for various combination between $q = 1, 1.5, 2$ and $\alpha_3 = 1, 5, 10$. There we find that as the magnitude of B_{0z} increases, first $Im(\beta)$ also increases and reaches a maximum value of 0.5⁶, and then it decreases. It also says that for a fixed α_3 , as q increases the domain of B_{0z} giving rise to positive $Im(\beta)$ decreases. On the other hand, for a fixed q the increment of α_3 decreases the window of B_{0z} , that gives rise to positive $Im(\beta)$. Between these effects of α_3 and q , the increment of α_3 for a fixed q affects the flow more severely.

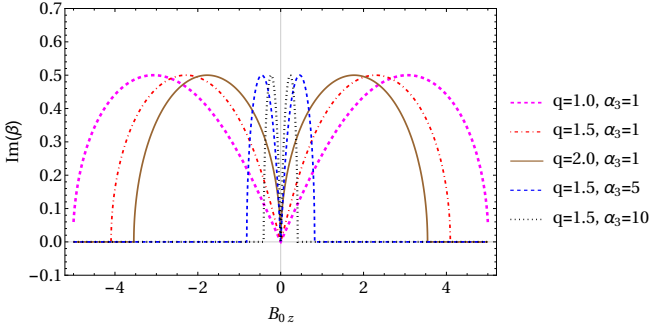


FIG. 1. Variation of $Im(\beta)$ of the unstable solution from equation (10) as a function of B_{0z} for various combinations of q and α_3 for inviscid flow.

IV. THE EFFECT OF EXTRA FORCE

In the presence of an extra force, vertical magnetic field and the vertical wavevector, equations (5a), (5b), (5c) and (5d) become

$$\begin{aligned} i\beta\alpha_3^2 u(0) + \frac{2i\alpha_3}{q}\zeta(0) + \frac{i\alpha_3^3 B_{0z} B_x(0)}{4\pi} &= m_1, \\ i\alpha_3 \left(1 - \frac{2}{q}\right) u(0) - i\beta\zeta(0) - \frac{i}{4\pi} B_{0z} \alpha_3 \zeta_B(0) &= m_2, \\ -i\beta B_x(0) - iB_{0z} \alpha_3 u(0) &= 0, \\ -i\beta \zeta_B(0) - iB_{0z} \alpha_3 \zeta(0) - i\alpha_3 B_x(0) &= 0. \end{aligned} \quad (13)$$

For simplicity, if we consider $m_1 = m_2 = m$ and write $u(0)$ as u_0 , the dispersion relation from equation (13) becomes

$$\begin{aligned} \frac{m}{u_0} (4\pi\alpha_3^2 B_{0z}^2 \beta - 16\pi^2 \beta^3) &= \frac{8i\pi B_{0z}^2 \alpha_3^4}{q} - i\alpha_3^6 B_{0z}^4 \\ + \frac{32\pi^2 \alpha_3 \beta^2}{q} \left(\frac{m}{u_0}\right) + \frac{64i\pi^2 \alpha_3^2 \beta^2}{q^2} - \frac{32i\pi^2 \alpha_3^2 \beta^2}{q} & \\ + 8i\pi\alpha_3^4 \beta^2 B_{0z}^2 - 16i\pi^2 \alpha_3^2 \beta^4. & \end{aligned} \quad (14)$$

A. Without magnetic field

To extract the hydrodynamical effect out of equation (14), we set $B_{0z} = 0$. Then the corresponding dispersion relation becomes

$$\begin{aligned} -i\alpha_3^2 \beta^2 + \frac{m}{u_0} \beta + \frac{2\alpha_3}{q} \left(\frac{m}{u_0}\right) + \frac{4i\alpha_3^2}{q^2} & \\ - \frac{2i\alpha_3^2}{q} &= 0. \end{aligned} \quad (15)$$

The solutions of this quadratic equation are

$$\beta = \frac{1}{2\alpha_3^2} \left[-i \left(\frac{m}{u_0}\right) \pm \sqrt{\frac{8\alpha_3^4}{q^2} (2-q) - \frac{m}{u_0} \left(\frac{m}{u_0} + \frac{8i\alpha_3^3}{q}\right)} \right]. \quad (16)$$

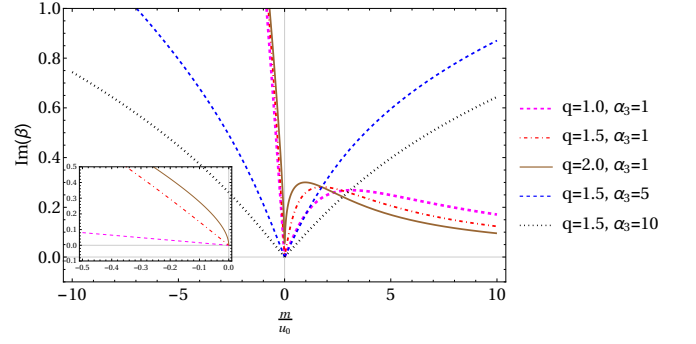


FIG. 2. Variation of $Im(\beta)$ of the unstable solution from equation (15) as a function of m/u_0 for various combinations of q and α_3 for inviscid flow.

If we compare equation (16) with equation (11), we notice the effect of noise on the stability of the flow. Equation (16) has two solutions. However, only one of them gives us positive $Im(\beta)$ as a function of m/u_0 , i.e., only that particular solution corresponds to instability in the flow. As we are interested in instability, we consider the first solution. In this case, the positive sign in front of the square root corresponds to the unstable solution.

FIG. 2 describes the variation of $Im(\beta)$ from equation (16) as a function of m/u_0 for various combinations of q and α_3 . Here we notice that for positive m/u_0 , when α_3 has been kept fixed, $Im(\beta)$ reaches a maximum and then it decreases. The maximum decreases as q decreases. Apart from that, the value of m/u_0 , at which the maximum in $Im(\beta)$ occurs, increases as q decreases. It, indeed, should be the case. Now for the negative m/u_0 , for the same case, it is obvious from the inset that the curve of larger q is steeper. It means that at each negative m/u_0 , larger q has larger $Im(\beta)$. This is what is expected. From equation (11), when the force is zero $q = 2$ gives the marginal stability and $q < 2$ makes the flow stable and the stability increases as the q becomes lesser than 2. Lesser q , therefore, takes larger force to make the flow unstable. For a fixed q , as α_3 increases, the curves become less steeper in most of the cases, hence at each m/u_0 lesser α_3 has larger growth rate [$Im(\beta)$]. This nature of the the growth rate for negative m/u_0 is quite obvious from the equation (16). However, for the positive m/u_0 , we notice that there will be a competition between the terms with and without square root in equation (16). As a result, for $\alpha_3 = 1$ and $q = 1.5$, we see that the growth rate increases as m/u_0 increases up to certain value of m/u_0 . Beyond that certain m/u_0 , the growth rate decreases.

B. With magnetic field

The equation (14) is a quartic equation. Here we look for the imaginary part of each root. Among the four solutions:

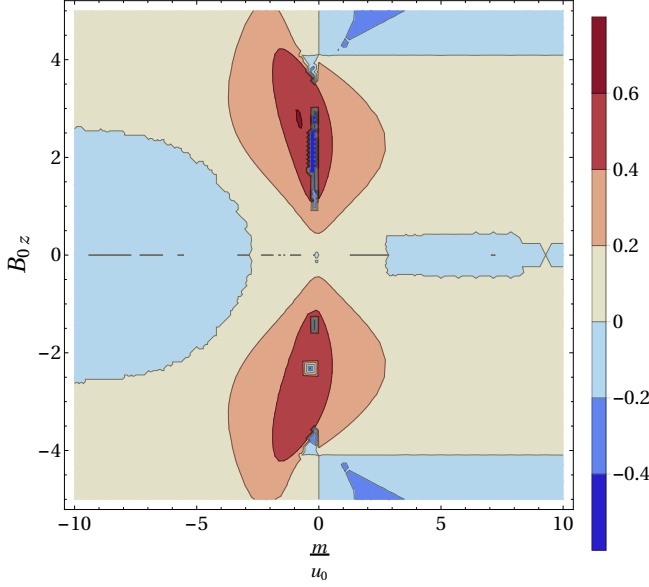


FIG. 3. Variation of $Im(\beta)$ of the ‘third solution’ of equation (14) as described in §IV B as a function of m/u_0 and B_{0z} for $q = 1.5$ and $\alpha_3 = 1$ for inviscid flow.

- the first and the fourth solutions together give us the solution given by equation (16) when magnetic field is switched off,
- the third solution gives us the MRI modes when noise is not there in the flow,
- the second solution gives us the stable modes corresponding to the MRI modes if the noise is made zero.

We will begin with the ‘third solution’ as it reduces to the usual MRI mode shown in FIG. 1, when there is no noise in the system.

1. The ‘third solution’

FIG. 3 describes the variation of $Im(\beta)$ as a function of m/u_0 and B_{0z} for $q = 1.5$ and $\alpha_3 = 1$. From FIG. 1 it is clear that for $q = 1.5$ and $\alpha_3 = 1$, the domain of B_{0z} that gives rise to positive $Im(\beta)$ is about within -4 to $+4$. To see what happens in that region of B_{0z} , we fix the range of the vertical axis in FIG. 3 within -5 to $+5$. We notice that the growth rate is mostly dominated by MRI in that region of the magnetic field. Around $m/u_0 = 0$, as the magnitude of B_{0z} increases, $Im(\beta)$ increases initially, reaches a maximum, and then again decays. Also, beyond a small region around $|m/u_0| = 0$, the flow is stable within the domain of m/u_0 as shown in the FIG. 3. However, the maximum growth rate shown in this figure is greater than MRI growth rate shown in FIG. 1. This could be due to the additional effect from the hydrodynamic instability because of the presence of noise in the flow.

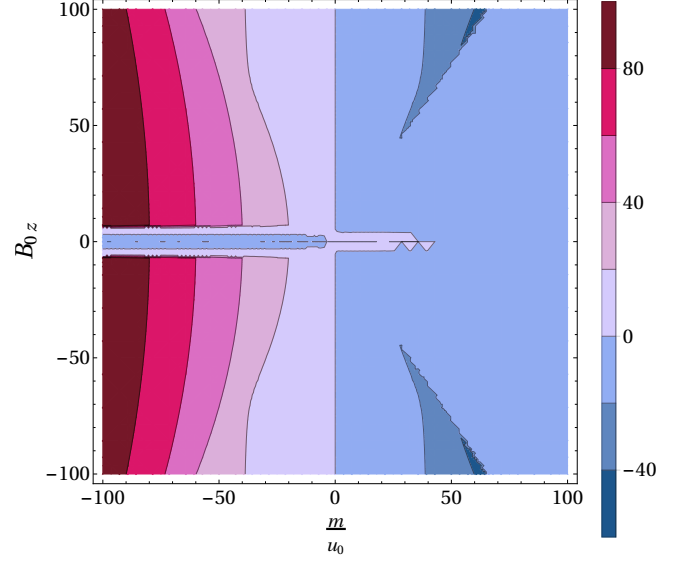


FIG. 4. Variation of $Im(\beta)$ of the ‘third solution’ of equation (14) as described in §IV B as a function of m/u_0 and B_{0z} in the larger domain for $q = 1.5$ and $\alpha_3 = 1$ for inviscid flow.

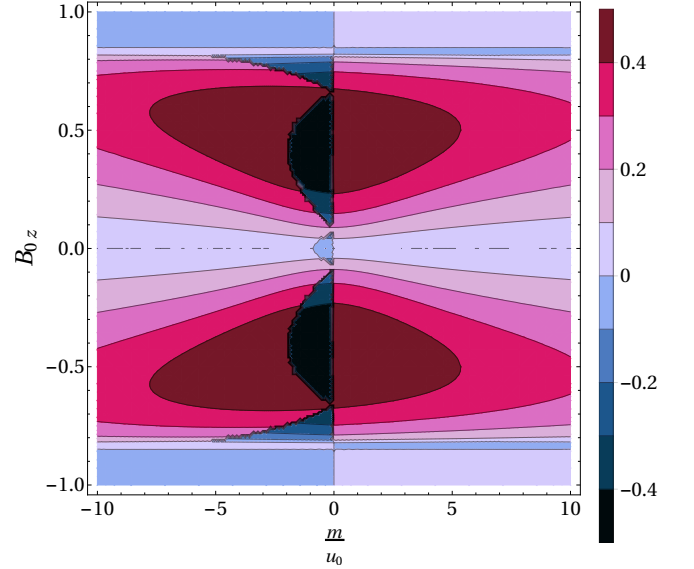


FIG. 5. Variation of $Im(\beta)$ of the ‘third solution’ of equation (14) as described in §IV B as a function of m/u_0 and B_{0z} in for $q = 1.5$ and $\alpha_3 = 5$ for inviscid flow.

Now, if we increase the domain of m/u_0 and B_{0z} , we notice that the flow is mostly stable for positive m/u_0 , but it is mostly unstable for negative m/u_0 as indicated by the FIG. 4, where the variation of $Im(\beta)$ is shown as a function of m/u_0 and B_{0z} in the larger domain. As the magnitude of m/u_0 increases, we notice that the growth rate increases. However, the positive growth rate becomes almost independent of the magnetic field at large m/u_0 . That is to say, at the larger magnetic field where

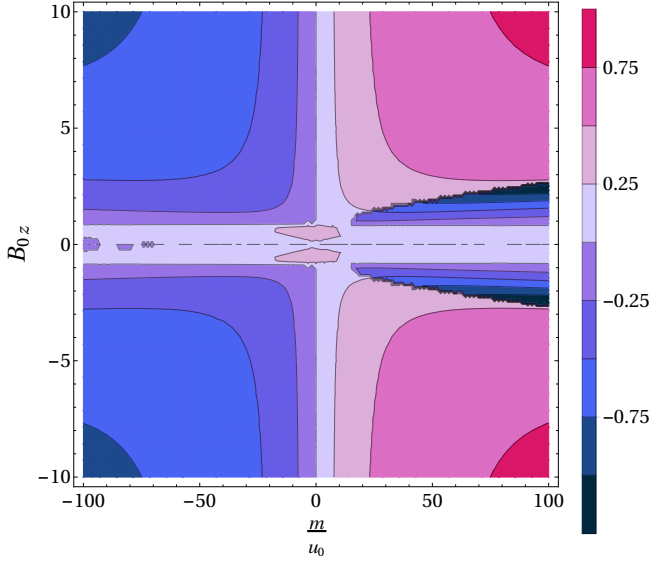


FIG. 6. Variation of $Im(\beta)$ of the ‘third solution’ of equation (14) as described in §IV B as a function of m/u_0 and B_{0z} in the larger domain for $q = 1.5$ and $\alpha_3 = 5$ for inviscid flow.

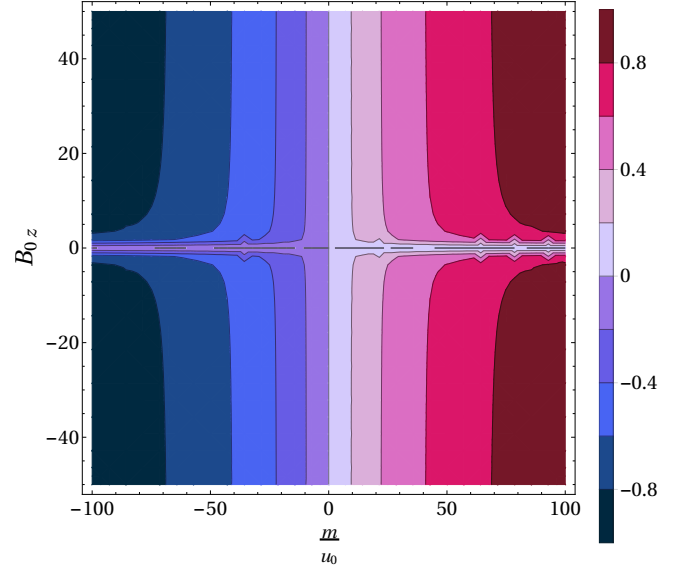


FIG. 8. Variation of $Im(\beta)$ of the ‘third solution’ of equation (14) as described in §IV B as a function of m/u_0 and B_{0z} in the larger domain for $q = 1.5$ and $\alpha_3 = 10$ for inviscid flow.

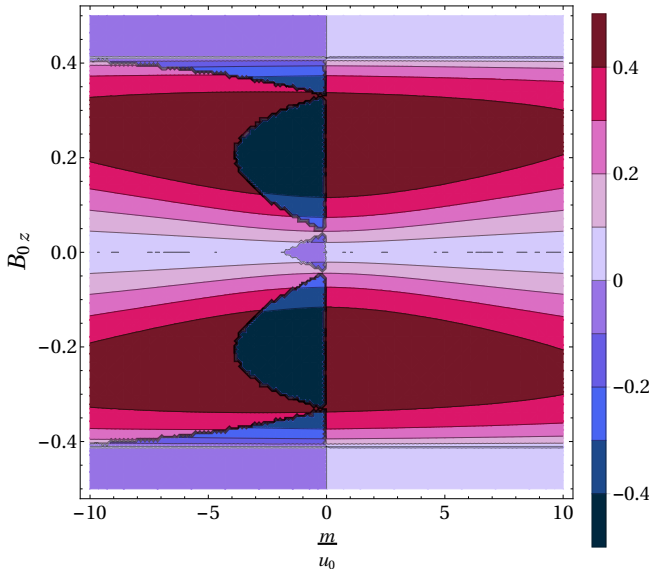


FIG. 7. Variation of $Im(\beta)$ of the ‘third solution’ of equation (14) as described in §IV B as a function of m/u_0 and B_{0z} for $q = 1.5$ and $\alpha_3 = 10$ for inviscid flow.

there is no growth due to MRI, the flow is mostly governed by the noise with huge growth rates.

Now, we increase α_3 to 5. FIG. 5 shows the variation of $Im(\beta)$ as a function of m/u_0 and B_{0z} for $q = 1.5$ and $\alpha_3 = 5$. From FIG. 1 we already have obtained that for $q = 1.5$ and $\alpha_3 = 5$, the window of B_{0z} that gives rise to positive $Im(\beta)$ is about within -1 to $+1$. We, therefore, keep the range of the vertical axis in FIG. 5 within ± 1 so that we can compare between MRI and instability due to noise. There we notice that the growth

rate is mostly governed by the MRI and the structure of the growth rate, i.e., how $Im(\beta)$ varies with B_{0z} at a particular m/u_0 , is also MRI-like. If we compare between the FIGS. 3 and 5, we observe that the range of $|m/u_0|$, that gives rise to a positive growth rate, increases as α_3 increases.

Now let us see what happens to the growth rates, when we extend the domain of m/u_0 and B_{0z} through the FIG. 6, where the variation of $Im(\beta)$ has been shown as a function of m/u_0 and B_{0z} for $q = 1.5$ and $\alpha_3 = 5$. There we notice that for negative m/u_0 , the flow is stable for any magnetic field. On the other hand, for positive m/u_0 , the flow is mostly unstable. However, there is a window of $-3 \lesssim B_{0z} \lesssim +3$, where the flow could be stable depending on m/u_0 . Here noise has the stabilizing effect because if we fix the magnetic field at any value within ± 3 , we notice that the flow suddenly becomes stable as we increase m/u_0 . However, in the unstable region, as the noise increases, the growth rate increases, and ultimately at large noise, the instability, due to the noise, takes over the flow. Thus, the regime of sterile magnetic field not leading to MRI, i.e. the strong field, turns out to be active in order to reveal instability in the presence of noise.

Now, we further increase α_3 to 10, which is in fact very much applicable to the accretion flow³⁷. FIG. 7 describes the variation of $Im(\beta)$ as a function of m/u_0 and B_{0z} for $q = 1.5$ and $\alpha_3 = 10$. We bound the vertical axis within ± 0.5 in this figure as FIG. 1 shows that the range of B_{0z} that gives rise to a positive growth rate is within around ± 0.5 . Here again, we notice that in this domain of magnetic field, the growth rate is mostly dominated by MRI. However, in comparison with the other two α_3 , for

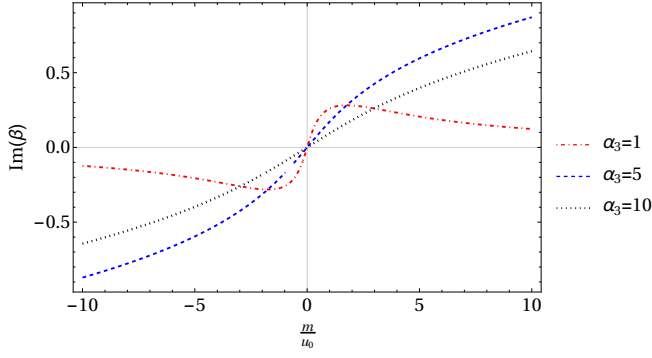


FIG. 9. Variation of $Im(\beta)$ of the ‘first solution’ of equation (14) as described in §IV B as a function of m/u_0 for $q = 1.5$ and three different α_3 when $B_{0z} = 0$ for inviscid flow.

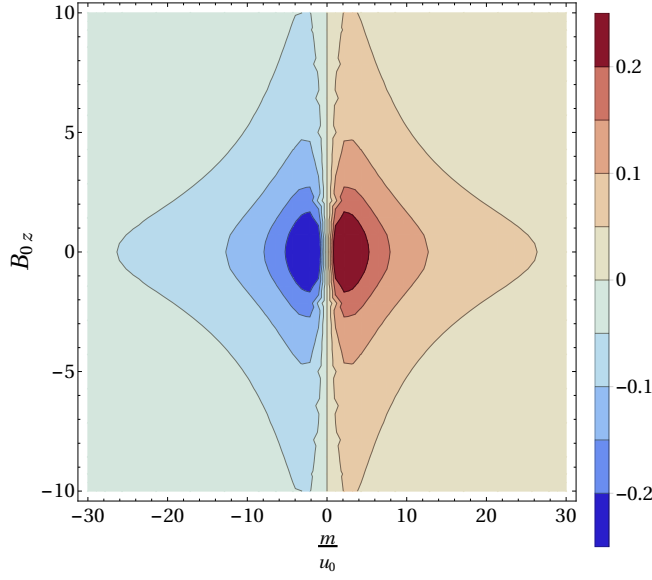


FIG. 10. Variation of $Im(\beta)$ of the ‘first solution’ of equation (14) as described in §IV B as a function of m/u_0 and B_{0z} for $q = 1.5$ and $\alpha_3 = 1$ for inviscid flow.

$\alpha_3 = 10$, the range of m/u_0 , which gives rise to a positive growth rate, is larger. Nevertheless, for the larger magnetic field, where MRI is inactive, the flow is again dominated by the instability due to the noise, particularly for positive m/u_0 . This phenomenon is well-depicted in the FIG. 8 which shows the variation of $Im(\beta)$ as a function of m/u_0 and B_{0z} in the larger domain for $q = 1.5$ and $\alpha_3 = 10$.

2. The ‘first solution’

The ‘first solution’ of $Im(\beta)$ from equation (14) as described in §IV B is shown in FIG. 9 for $B_{0z} = 0$ and three different α_3 . There we notice that the variation of $Im(\beta)$ for positive m/u_0 is the same as of FIG. 2 for positive m/u_0 . We see that up to certain positive m/u_0 ,

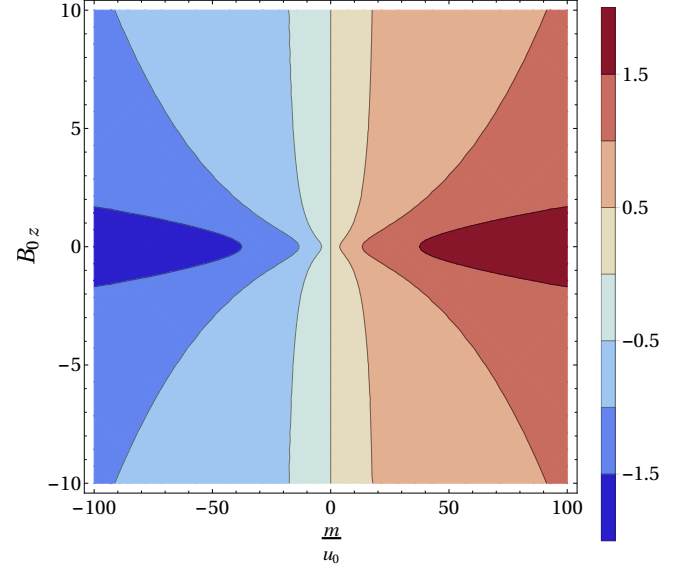


FIG. 11. Variation of $Im(\beta)$ of the ‘first solution’ of equation (14) as described in §IV B as a function of m/u_0 and B_{0z} for $q = 1.5$ and $\alpha_3 = 5$ for inviscid flow.

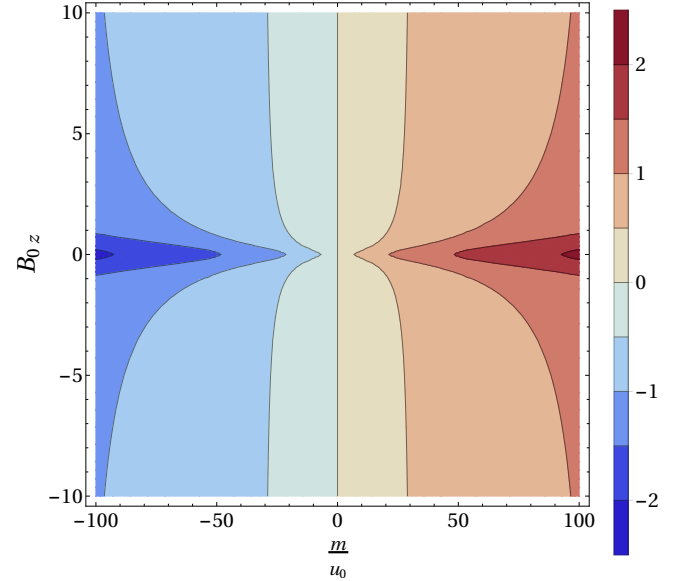


FIG. 12. Variation of $Im(\beta)$ of the ‘first solution’ of equation (14) as described in §IV B as a function of m/u_0 and B_{0z} for $q = 1.5$ and $\alpha_3 = 10$ for inviscid flow.

the growth rates corresponding to the smaller α_3 increase steeply. However, beyond that m/u_0 , the growth rate decreases. The similar feature is depicted in FIG. 10 where the variation of the growth rate is shown a function of m/u_0 and B_{0z} for $\alpha_3 = 1$. However, for a particular m/u_0 , we see that the growth rate decreases with the increase of the magnitude of B_{0z} . Hence, in this case, the magnetic field affects the flow destructively with the effect of noise.

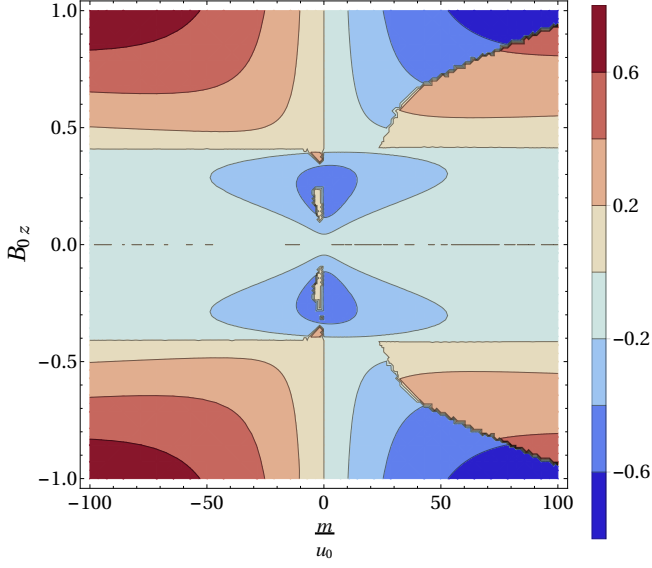


FIG. 13. Variation of $Im(\beta)$ of the ‘second solution’ of equation (14) as described in §IV B as a function of m/u_0 and B_{0z} for $q = 1.5$ and $\alpha_3 = 10$ for inviscid flow.

FIGs. 11 and 12 show the variation of $Im(\beta)$ of the ‘first solution’ of equation (14) as described in §IV B as a function of m/u_0 and B_{0z} for $q = 1.5$, for $\alpha_3 = 5$ and 10, respectively. There we notice that the growth rates for these two cases are similar to that in the FIG. 10. Within a very small domain of magnetic field, for a fixed m/u_0 , the growth rate decreases with the increase in the magnitude of the magnetic field. Beyond that domain of B_{0z} , the growth rate is almost independent of magnetic field. However, the domain of magnetic field, in which the growth rate depends on the magnetic field, shrinks in size as α_3 increases to 10 from 5. It could plausibly be because nonzero noise effectively brings in MRI-like features, i.e. the decrease in size of the MRI active magnetic field regime due to the increase in wavevector, for a particular region of magnetic field.

The maximum growth rate in FIG. 12, is relatively larger than that in FIG. 8. Note that both of these figures have the same α_3 and the same range of m/u_0 . While FIG. 8 represents the ‘third solution’ for a given set of parameters, FIG. 12 represents the ‘first solution’ for the concerned parameters. The latter one, being solely hydrodynamical, does not have any MRI counterpart. On the contrary, the former one does reduce to the MRI solution at the vanishing noise.

3. The ‘second solution’

The ‘second solution’ of equation (14) is stable version of the third solution of the same equation if there is no noise in the flow. FIG. 13 shows the variation of $Im(\beta)$ of the second solution of equation (14) as a function of

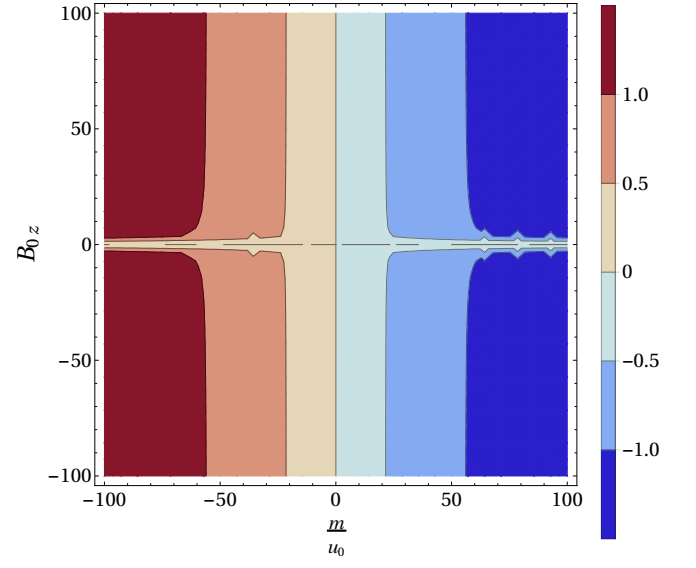


FIG. 14. Variation of $Im(\beta)$ of the ‘second solution’ of equation (14) as described in §IV B as a function of m/u_0 and B_{0z} in the larger domain for $q = 1.5$ and $\alpha_3 = 10$ for inviscid flow.

m/u_0 and B_{0z} for $q = 1.5$ and $\alpha_3 = 10$. FIG. 14 also depicts the same but in the larger domain of m/u_0 and B_{0z} . We notice that FIG. 13 is almost complementary to the FIG. 6. Within a certain domain of B_{0z} , the flow is stable, and the stability arises due to the domination of the magnetic field over the effect of noise. However, beyond that particular domain of B_{0z} , the flow becomes unstable due the effect of noise. For negative m/u_0 , we notice that beyond certain magnetic field, the growth rate increases as the magnitude of m/u_0 increases. In this region, the growth rate increases with the increase of magnitude of both m/u_0 and B_{0z} . However, at the larger magnetic field, the flow is almost controlled by the noise particularly with negative mean. We are also familiar with similar invasion of noise but with positive mean in case of the third solution described in IV B 1.

4. The ‘fourth solution’

The ‘fourth solution’ of equation (14) is almost complementary solution to the first solution of the same equation. However, there is some difference, i.e., they are not exactly the complex conjugate as the coefficients of equation (14) are complex quantities. It will be understood if we go through FIG. 15, which describes variation of $Im(\beta)$ of the fourth solution of equation (14) as a function of m/u_0 and B_{0z} in the larger domain for $q = 1.5$ and $\alpha_3 = 10$. Here we notice that for negative m/u_0 , the growth rate is positive. For smaller m/u_0 , as the magnitude of the magnetic field increases, only up to certain range of the magnetic field, the growth rate increases. However, for the larger m/u_0 , the above phe-

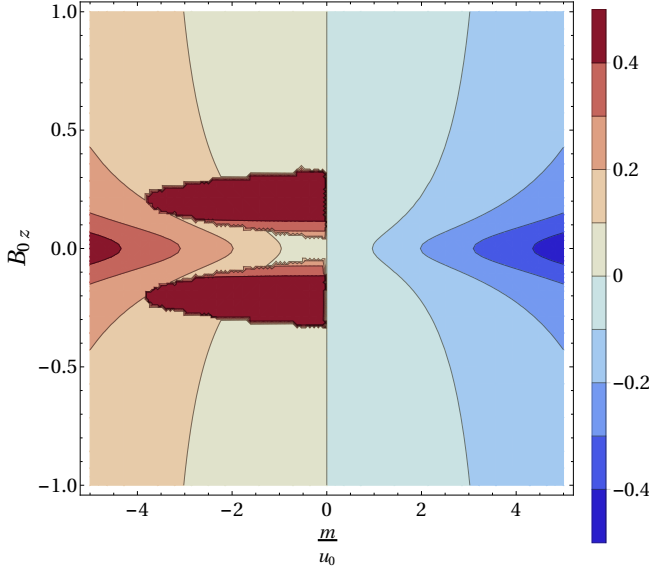


FIG. 15. Variation of $Im(\beta)$ of the ‘fourth solution’ of equation (14) as described in §IV B as a function of m/u_0 and B_{0z} for $q = 1.5$ and $\alpha_3 = 10$ for inviscid flow.

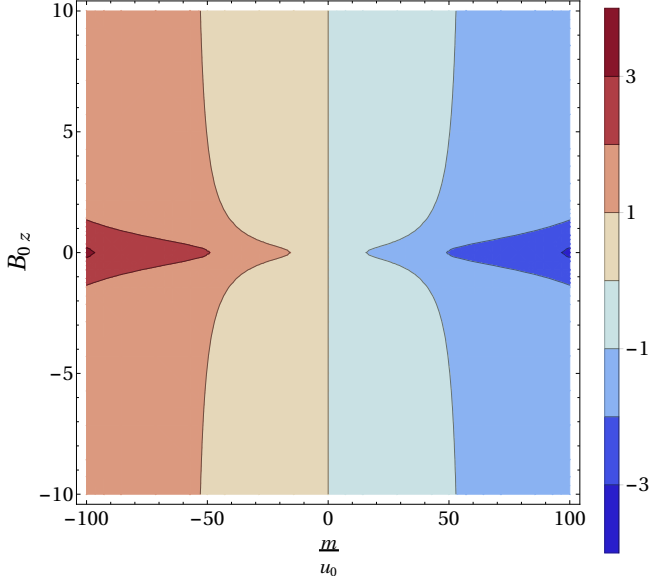


FIG. 16. Variation of $Im(\beta)$ of the ‘fourth solution’ of equation (14) as described in §IV B as a function of m/u_0 and B_{0z} in the larger range for $q = 1.5$ and $\alpha_3 = 10$ for inviscid flow.

nomenon reverses, i.e., as the magnitude of the magnetic field increases, the flow becomes less unstable. Now, for the larger ranges of m/u_0 and B_{0z} , as described by the FIG. 16 it is the noise that takes over the flow. Consequently, the instability in the flow arises due to the noise.

V. THE EFFECT OF Re

Till now, we have not considered the effect of viscous dissipation. Let us explore the effect of the same on the growth rates. Consequently, the equation (13) becomes,

$$\begin{aligned} \left(i\beta\alpha_3^2 - \frac{\alpha^4}{Re}\right)u(0) + \frac{2i\alpha_3}{q}\zeta(0) + \frac{i\alpha_3^3 B_{0z} B_x(0)}{4\pi} &= m_1, \\ i\alpha_3 \left(1 - \frac{2}{q}\right)u(0) + \left(\frac{\alpha^2}{Re} - i\beta\right)\zeta(0) - \frac{i}{4\pi}B_{0z}\alpha_3\zeta_B(0) &= m_2, \\ -i\beta B_x(0) - iB_{0z}\alpha_3 u(0) &= 0, \\ -i\beta\zeta_B(0) - iB_{0z}\alpha_3\zeta(0) - i\alpha_3 B_x(0) &= 0. \end{aligned} \quad (17)$$

The corresponding dispersion relation for $m_1 = m_2 = m$ from equation (17) becomes,

$$\begin{aligned} \frac{m}{u_0} \left(4\pi\alpha_3^2 B_{0z}^2 \beta - \frac{16i\pi^2 \alpha_3^2 \beta^2}{Re} - 16\pi^2 \beta^3\right) &= \frac{8i\pi B_{0z}^2 \alpha_3^4}{q} \\ -i\alpha_3^6 B_{0z}^4 + \frac{32\pi^2 \alpha_3 \beta^2}{q} \left(\frac{m}{u_0}\right) + \frac{64i\pi^2 \alpha_3^2 \beta^2}{q^2} \\ - \frac{32i\pi^2 \alpha_3^2 \beta^2}{q} + 8i\pi\alpha_3^4 \beta^2 B_{0z}^2 + \frac{16i\pi^2 \alpha_3^6 \beta^2}{Re^2} + \frac{32\pi^2 \alpha_3^4 \beta^3}{Re} \\ - 16i\pi^2 \alpha_3^2 \beta^4. \end{aligned} \quad (18)$$

If the magnetic field is not there in the system, then the above dispersion relation becomes,

$$\begin{aligned} -i\alpha_3^2 \beta^2 + \left(\frac{2\alpha_3^4}{Re} + \frac{m}{u_0}\right)\beta + \frac{2\alpha_3}{q} \left(\frac{m}{u_0}\right) \\ + \frac{4i\alpha_3^2}{q^2} - \frac{2i\alpha_3^2}{q} + \frac{i\alpha_3^2}{Re} \left(\frac{m}{u_0}\right) + \frac{i\alpha_3^6}{Re^2} = 0 \end{aligned} \quad (19)$$

with the solutions

$$\begin{aligned} \beta = \\ \frac{1}{2\alpha_3^2} \left[-i \left(\frac{m}{u_0}\right) - \frac{2i\alpha_3^4}{Re} \pm \sqrt{\frac{8\alpha_3^4}{q^2} (2-q) - \frac{m}{u_0} \left(\frac{m}{u_0} + \frac{8i\alpha_3^3}{q}\right)} \right]. \end{aligned} \quad (20)$$

If we compare equation (16) with equation (20), we notice that the latter has an additional term involving Re . Since, the term is imaginary, it reduces the instability in the flow. Hence, inclusion of Re makes the flow less unstable if there is no effect of magnetic field in the flow. Equation (19) is same as equation (9) in Nath and Mukhopadhyay³⁵. Figure 2 in Nath and Mukhopadhyay³⁵ also suggests that inclusion of Re , decreases the growth rate.

Let us incorporate the magnetic field in the flow and get rid of the effect of noise. Then we obtain the usual MRI but with the affect of viscosity. FIG. 17 shows the variation of $Im(\beta)$ of the third solution of equation (18)

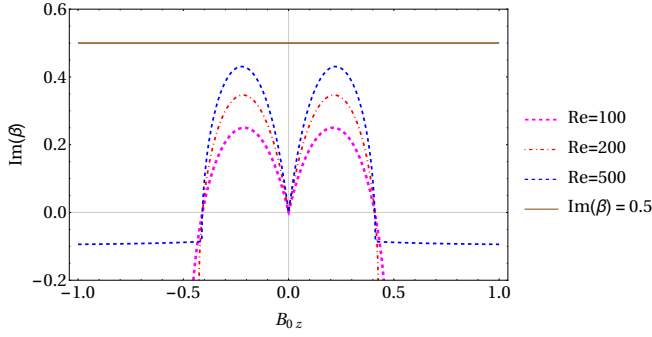


FIG. 17. Variation of $Im(\beta)$ of the third solution of equation (18) when $m = 0$ as a function of B_{0z} for $q = 1.5$, $\alpha_3 = 10$ and $Re = 100, 200$ and 500 .

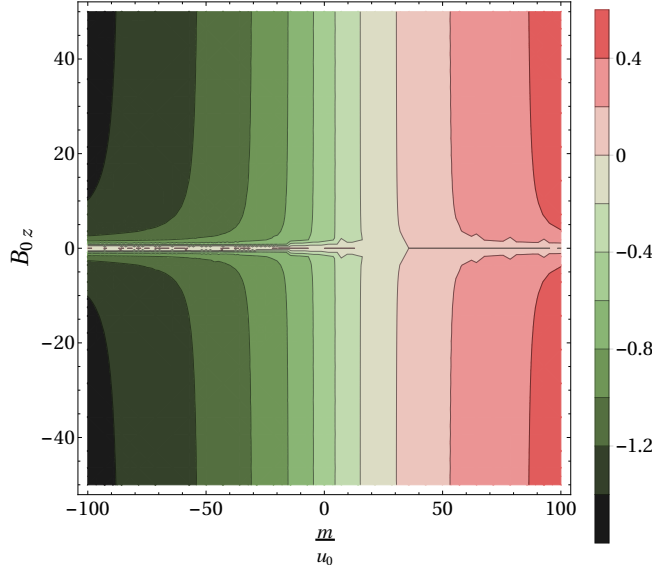


FIG. 18. Variation of $Im(\beta)$ of the third solution of equation (18) as a function of m/u_0 and B_{0z} for $q = 1.5$, $\alpha_3 = 10$ and $Re = 100$.

when $m = 0$ as a function of B_{0z} for $q = 1.5$, $\alpha_3 = 10$ and $Re = 100, 200$ and 500 . This figure shows that with the inclusion of viscosity i.e. Re in the flow, the growth rate decreases. As Re increases the corresponding growth rates also increase and ultimately reach the results of inviscid limit. This phenomenon becomes obvious once we compare between the FIGs. 17 and 1. Let us study the effect of Re on the growth rate if both magnetic field and the noise are present in the flow. FIG. 18 shows the variation of $Im(\beta)$ of the third solution of equation (18) as a function of m/u_0 and B_{0z} for $q = 1.5$, $\alpha_3 = 10$ and $Re = 100$. If we compare between FIGs. 8 and 18, we notice that in the later case the growth rate decreases due to considering the viscosity, i.e. Re in the flow.

FIG. 19 shows the variation of $Im(\beta)$ of the first solution of equation (18) as a function of m/u_0 and B_{0z} for $q = 1.5$, $\alpha_3 = 10$ and $Re = 50$. If we compare it with FIG. 12, we notice that the growth rate becomes nega-

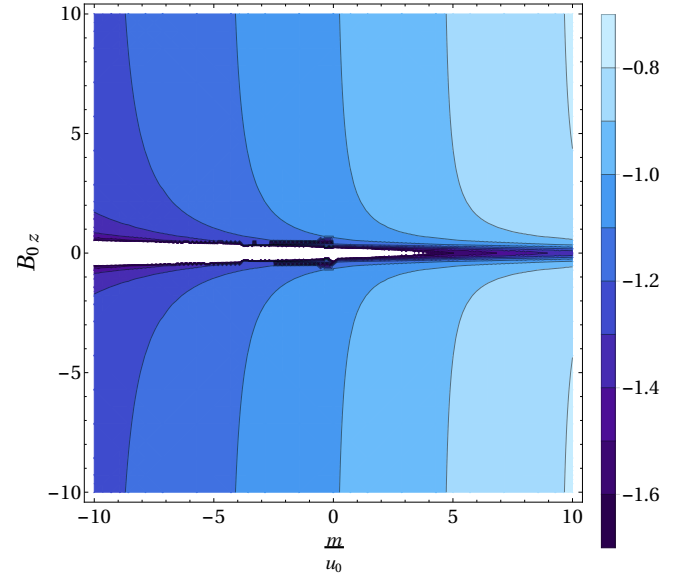


FIG. 19. Variation of $Im(\beta)$ of the first solution of equation (18) as a function of m/u_0 and B_{0z} for $q = 1.5$, $\alpha_3 = 10$ and $Re = 50$.

tive, i.e. the flow becomes stable, for $Re = 50$. However, as Re increases, the growth rates increases and eventually at large Re , FIG. 19 becomes FIG. 12. Now, $Im(\beta)$ for the second and fourth solutions of equation(18), also get reduced due the presence of the viscosity, i.e. Re .

VI. CONCLUSION

The transport of angular momentum outward and that of the matter inward in the accretion disk is still debatable and arguably open question till today, particularly at the low-temperature region of the accretion disks. In the hot region, MRI is quite successful in explaining the transport. However, there are different parameter regimes (e.g., large magnetic field and huge Reynolds number¹⁴, a large toroidal component of the magnetic field¹³, etc.) where MRI gets suppressed or ceases to work. In the previous publications^{36–38}, we attempted to propose a generic instability mechanism from the hydrodynamical point of view if noise is present in the corresponding flow. With that thought, here we have attempted to compare the growth rates corresponding to both the mechanisms. We have attempted to check what happens to the growth rates if both magnetic field as well as the noise with non-zero mean is present in the flow. From the analysis, our conclusions are following.

- Among the four solutions for the growth rates, one of them reduces to the MRI growth rate if the noise is absent. If both noise as well as the magnetic field are present in the flow, in the MRI active region of the magnetic field, the growth rates follow the MRI growth rate pattern, i.e., the growth rate first

increases, attains a maximum, and then again decreases with the variation of magnetic field. However, the corresponding maximum growth rate is slightly larger than the MRI growth rate. In the larger domain of magnetic field where MRI is inactive, the instability is almost entirely due to the noise as the corresponding growth rates are almost independent of the magnetic field. However, there is another growth rate which is almost complementary to the above mentioned growth rate.

- Further, there is another solution for the growth rate which reduces to the growth rate related to the hydrodynamic instability due to the presence of noise in the flow when the magnetic field is absent. This solution has nothing to do with MRI. When both magnetic field and noise are retained in the flow, at the MRI active magnetic field region also the growth rate is larger than that of the MRI. This growth rate does not have any MRI imprint. The magnitude of the growth rate mostly depends on the mean of the noise. As the mean increases, the growth rate increases. However, this also has an almost complimentary growth rate, which is the last solution in the set of four.
- Above points summarize that even in the MRI active region, as there are two growth rates which are larger at the comparatively larger mean of the noise than those of the other two solutions which have the imprint of MRI, the corresponding flow becomes unstable due to the hydrodynamical instability in the presence of noise.
- All the growth rates decrease due to the presence of viscosity in the flow. As the Reynolds number increases, the corresponding growth rates increase, as expected.

ACKNOWLEDGEMENT

S.G. thanks DST India for INSPIRE fellowship. We want to thank Prof. Vinod Krishan of the Indian Institute of Astrophysics for her constructive comments and suggestions that help to shape our thoughts in better ways. This work is partly supported by a fund of the Department of Science and Technology (DST-SERB) with research Grant No. DSTO/PPH/BMP/1946 (EMR/2017/001226) and a fund of the Indian Institute of Science.

¹J. Frank, A. King, and D. J. Raine, *Accretion Power in Astrophysics*, by Juhan Frank and Andrew King and Derek Raine, pp. 398. ISBN 0521620538. Cambridge, UK: Cambridge University Press, February 2002. (2002) p. 398.

²N. I. Shakura and R. A. Sunyaev, "Black holes in binary systems. Observational appearance," *Astron. Astrophys.* **24**, 337–355 (1973).

- ³S. A. Balbus and J. F. Hawley, "A powerful local shear instability in weakly magnetized disks. I - Linear analysis. II - Nonlinear evolution," *Astrophys. J.* **376**, 214–233 (1991).
- ⁴E. Velikhov, "Stability of an ideally conducting liquid flowing between rotating cylinders in a magnetic field," *Zhur. Eksptl'. i Teoret. Fiz.* **Vol: 36** (1959).
- ⁵S. Chandrasekhar, "The Stability of Non-Dissipative Couette Flow in Hydromagnetics," *Proceedings of the National Academy of Science* **46**, 253–257 (1960).
- ⁶S. A. Balbus and J. F. Hawley, "Instability, turbulence, and enhanced transport in accretion disks," *Reviews of Modern Physics* **70**, 1–53 (1998).
- ⁷C. F. Gammie, "Layered Accretion in T Tauri Disks," *Astrophys. J.* **457**, 355 (1996).
- ⁸T. Fleming and J. M. Stone, "Local Magnetohydrodynamic Models of Layered Accretion Disks," *Astrophys. J.* **585**, 908–920 (2003), arXiv:astro-ph/0210541 [astro-ph].
- ⁹N. J. Turner, S. Fromang, C. Gammie, H. Klahr, G. Lesur, M. Wardle, and X. N. Bai, "Transport and Accretion in Planet-Forming Disks," in *Protostars and Planets VI*, edited by H. Beuther, R. S. Klessen, C. P. Dullemond, and T. Henning (2014) p. 411, arXiv:1401.7306 [astro-ph.EP].
- ¹⁰X.-N. Bai and J. M. Stone, "Wind-driven Accretion in Protoplanetary Disks. I. Suppression of the Magnetorotational Instability and Launching of the Magnetocentrifugal Wind," *Astrophys. J.* **769**, 76 (2013), arXiv:1301.0318 [astro-ph.EP].
- ¹¹X.-N. Bai, "Wind-driven Accretion in Protoplanetary Disks. II. Radial Dependence and Global Picture," *Astrophys. J.* **772**, 96 (2013), arXiv:1305.7232 [astro-ph.EP].
- ¹²M. E. Pessah and D. Psaltis, "The Stability of Magnetized Rotating Plasmas with Superthermal Fields," *Astrophys. J.* **628**, 879–901 (2005), astro-ph/0406071.
- ¹³U. Das, M. C. Begelman, and G. Lesur, "Instability in strongly magnetized accretion discs: A global perspective," *Mon. Not. Roy. Astron. Soc.* **473**, 2791–2812 (2018), arXiv:1709.09173 [astro-ph.HE].
- ¹⁴S. K. Nath and B. Mukhopadhyay, "Origin of nonlinearity and plausible turbulence by hydromagnetic transient growth in accretion disks: Faster growth rate than magnetorotational instability," *Phys. Rev. E* **92**, 023005 (2015), arXiv:1505.02874 [astro-ph.HE].
- ¹⁵B. Mukhopadhyay and A. K. Chattopadhyay, "Stochastically driven instability in rotating shear flows," *Journal of Physics A Mathematical General* **46**, 035501 (2013), arXiv:1211.5135 [astro-ph.HE].
- ¹⁶S. Chandrasekhar, *Hydrodynamic and hydromagnetic stability* (1961).
- ¹⁷L. D. Landau and E. M. Lifshitz, *Fluid mechanics* (1959).
- ¹⁸D. Richard and J.-P. Zahn, "Turbulence in differentially rotating flows what can be learned from the couette-taylor experiment," *Astron. Astrophys.* **347**, 734 (1999), arXiv:astro-ph/9903374 [astro-ph].
- ¹⁹D. P. M. van Gils, G.-W. Bruggert, D. P. Lathrop, C. Sun, and D. Lohse, "The twente turbulent taylor-couette (t3c) facility: Strongly turbulent (multiphase) flow between two independently rotating cylinders," *Review of Scientific Instruments* **82**, 025105 (2011), <https://doi.org/10.1063/1.3548924>.
- ²⁰M. S. Paoletti and D. P. Lathrop, "Angular momentum transport in turbulent flow between independently rotating cylinders," *Phys. Rev. Lett.* **106**, 024501 (2011).
- ²¹Paoletti, M. S., van Gils, D. P. M., Dubrulle, B., Sun, Chao, Lohse, Detlef, and Lathrop, D. P., "Angular momentum transport and turbulence in laboratory models of keplerian flows," *A&A* **547**, A64 (2012).
- ²²H. Ji, M. Burin, E. Scharfman, and J. Goodman, "Hydrodynamic turbulence cannot transport angular momentum effectively in astrophysical disks," *Nature (London)* **444**, 343–346 (2006), arXiv:astro-ph/0611481 [astro-ph].
- ²³S. Fromang and G. Lesur, "Angular momentum transport in accretion disks: a hydrodynamical perspective," in *EAS Publica-*

- tions Series, EAS Publications Series, Vol. 82 (2019) pp. 391–413.
- ²⁴M. Avila, “Stability and Angular-Momentum Transport of Fluid Flows between Corotating Cylinders,” *Physical Review Letters* **108**, 124501 (2012), arXiv:1203.4923 [physics.flu-dyn].
- ²⁵Tevzadze, A. G., Chagelishvili, G. D., Zahn, J.-P., Chanishvili, R. G., and Lominadze, J. G., “On hydrodynamic shear turbulence in stratified keplerian disks: Transient growth of small-scale 3d vortex mode perturbations,” *A&A* **407**, 779–786 (2003).
- ²⁶Chagelishvili, G. D., Zahn, J.-P., Tevzadze, A. G., and Lominadze, J. G., “On hydrodynamic shear turbulence in keplerian disks: Via transient growth to bypass transition,” *A&A* **402**, 401–407 (2003).
- ²⁷Yecko, P. A., “Accretion disk instability revisited - transient dynamics of rotating shear flow,” *A&A* **425**, 385–393 (2004).
- ²⁸B. Mukhopadhyay, N. Afshordi, and R. Narayan, “Bypass to Turbulence in Hydrodynamic Accretion Disks: An Eigenvalue Approach,” *Astrophys. J.* **629**, 383–396 (2005), astro-ph/0412193.
- ²⁹N. Afshordi, B. Mukhopadhyay, and R. Narayan, “Bypass to Turbulence in Hydrodynamic Accretion: Lagrangian Analysis of Energy Growth,” *Astrophys. J.* **629**, 373–382 (2005), astro-ph/0412194.
- ³⁰P. A. Schmid, D. A. Henningson, and D. R. Jankowski, “Stability and Transition in Shear Flows,” *Applied Mechanics Reviews* **55**, B57–B59 (2002), https://asmedigitalcollection.asme.org/appliedmechanicsreviews/article-pdf/55/3/B57/5438781/b41_1.pdf.
- ³¹Lesur, G. and Longaretti, P.-Y., “On the relevance of subcritical hydrodynamic turbulence to accretion disk transport,” *A&A* **444**, 25–44 (2005).
- ³²L. Shi, B. Hof, M. Rampp, and M. Avila, “Hydrodynamic turbulence in quasi-Keplerian rotating flows,” *Physics of Fluids* **29**, 044107 (2017), arXiv:1703.01714 [physics.flu-dyn].
- ³³P. J. Ioannou and A. Kakouris, “Stochastic Dynamics of Keplerian Accretion Disks,” *Astrophys. J.* **550**, 931–943 (2001).
- ³⁴D. N. Razdoburdin, “Perturbation dynamics in Keplerian flow under external stochastic forcing,” *Monthly Notices of the Royal Astronomical Society* **492**, 5366–5376 (2020), <https://academic.oup.com/mnras/article-pdf/492/4/5366/32465475/staa145.pdf>.
- ³⁵S. K. Nath and B. Mukhopadhyay, “A Pure Hydrodynamic Instability in Shear Flows and Its Application to Astrophysical Accretion Disks,” *Astrophys. J.* **830**, 86 (2016), arXiv:1608.00980 [astro-ph.HE].
- ³⁶S. Ghosh and B. Mukhopadhyay, “Hydrodynamical instability with noise in the Keplerian accretion discs: modified Landau equation,” *Monthly Notices of the Royal Astronomical Society* **496**, 4191–4208 (2020), <https://academic.oup.com/mnras/article-pdf/496/4/4191/33498503/staa1780.pdf>.
- ³⁷S. Ghosh and B. Mukhopadhyay, “Origin of hydrodynamic instability from noise: From laboratory flow to accretion disk,” *Physical Review Fluids* **6**, 013903 (2021), arXiv:2012.13417 [astro-ph.HE].
- ³⁸S. Ghosh and B. Mukhopadhyay, “Forced linear shear flows with rotation: rotating Couette-Poiseuille flow, its stability and astrophysical implications,” arXiv e-prints, arXiv:2107.04012 (2021), arXiv:2107.04012 [physics.flu-dyn].
- ³⁹T. Singh Bhatia and B. Mukhopadhyay, “Exploring non-normality in magnetohydrodynamic rotating shear flows: Application to astrophysical accretion disks,” *Physical Review Fluids* **1**, 063101 (2016), arXiv:1609.01841 [astro-ph.HE].
- ⁴⁰B. Mukhopadhyay, R. Mathew, and S. Raha, “Growing pseudo-eigenmodes and positive logarithmic norms in rotating shear flows,” *New Journal of Physics* **13**, 023029 (2011), arXiv:1101.4608 [astro-ph.HE].
- ⁴¹P. G. Drazin and W. H. Reid, *Hydrodynamic Stability*, by P. G. Drazin and W. H. Reid, pp. 626. ISBN 0521525411. Cambridge, UK: Cambridge University Press, September 2004. (2004) p. 626.